Validation of sensitivity and reliability of GPR and microgravity detection of underground cavities in complex urban settings: Test case of a cellar

Jakub CHROMČÁK[1], Michal GRINČ[2,3], Jaroslava PÁNISOVÁ[2,*], Peter VAJDA[2], Anna KUBOVÁ[2]

[1] Department of Geodesy, University of Žilina in Žilina, Slovak Republic

[2] Earth Science Institute, Slovak Academy of Sciences,
   Dúbravská cesta 9, 845 28 Bratislava, Slovak Republic;
   e-mail: geofjapa@savba.sk, tel.: +421 2 59410 603, fax: +421 2 59410 607

[3] Research centre of the University of Žilina, University of Žilina in Žilina, Slovak Republic

Abstract: We test here the feasibility of ground-penetrating radar (GPR) and microgravity methods in identifying underground voids, such as cellars, tunnels, abandoned mine-workings, etc., in complex urban conditions. For this purpose, we selected a cellar located under a private lot in a residential quarter of the town of Senec in Western Slovakia, which was discovered by chance when a small sinkhole developed on the yard just two meters away from the house. The size of our survey area was limited 1) by the presence of a technical room built at the back of the yard with a staircase leading to the garden, and 2) by the small width of the lot. Therefore the geophysical survey was carried out only in the backyard of the lot as we were not permitted to measure on neighbouring estates. The results from the GPR measurements obtained by the GSSI SIR-3000 system with 400 MHz antenna were visualized in the form of 2D radargrams with the corresponding transformed velocity model of studied cross-sections. Only the profiles running over the pavement next to the house yielded interpretable data because the local geological situation and the regular watering of the lawn covering prevailingly the backyard caused significant attenuation of the emitted GPR signal. The Bouguer gravity map is dominated by a distinctive negative anomaly indicating the presence of a shallow underground void. The quantitative interpretation by means of Euler deconvolution was utilized to validate the depth of the center and location of the cellar. Comparison with the gravitational effect of the cellar model calculated in the in-house program Polygrav shows a quite good correlation between the modelled and observed fields. Only a part of the aerial extent of the anomaly could be traced by the used geophysical methods due to accessibility issues. Nevertheless, the test cellar was successfully detected and interpreted by both methods, thus confirming their applicability in similar environmental and geotechnical applications, even in complex urban conditions.

---

*corresponding author

1. Introduction

The investigation of underground natural or man-made cavities and associated areas of soft ground in urban areas is of great importance, as their presence can often lead to subsidence-related problems for the land users, and also constitutes a potential hazard in industrialized zones. The most common natural targets include limestone solution-related features, underground drainage channels, caves and sinkholes. Abandoned constructed features of human action origin, such as old cellars, tunnels, shafts or mines, can be discovered during the site redevelopment and cause expensive delays in construction projects (e.g., *Al-Rifaiy, 1990; Styles et al., 2006; Tuckwell et al., 2008*).

Whilst the physical properties of both natural and man-made cavities are the same, there are differences in the properties of the host rock. If the natural cavity originates from the physical and chemical action of ground water on the rock, the surrounding material is often undisturbed. On the other hand, fracturing typical for man-made cavities usually increases its effective geophysical size up to several diameters. This cavity enhancement also termed as a halo effect is a function of cavity size, the strength of the rock, excavation technique and position of the water table (*Daniels, 1988*).

Non-invasive, indirect geophysical prospecting methods, including electrical resistivity, induced polarization, electromagnetic, GPR, seismic and gravimetry, have been successfully employed for the detection of near-surface cavities in geohazard applications over the last decades. Geophysical surveys carried out in urban areas are often limited by infrastructure and noise due to human activities. In such cases, an integrated approach combining advantages of several properly selected methods, considering the local geology and site conditions, help to reduce the degree of ambiguity (e.g., *Banham and Pringle, 2011; Cardarelli et al., 2010; Negri et al., 2015*).

The microgravity method is based on highly accurate measurement and interpretation of very small variations in Earth's gravitational field. Geological noise in traditional gravity prospecting becomes a useful signal in microgravity surveys and vice versa. The depth of investigation is related

to feature size and density contrast with respect to their surroundings. The microgravity method is a good indicator of air-filled cavities in the shallow subsurface and it is usable in virtually all environments, even indoors (*Pánisová et al., 2012; Styles et al., 2005*). However, it is limited by inherent ambiguity in interpretation and by slow daily production.

The GPR uses high frequency electromagnetic waves, which are transmitted into the subsurface and scattered and/or reflected back to a receiving antenna from interfaces and objects of different electrical properties. Spatial resolution and depth penetration of GPR depends on antenna frequency being used, propagation velocities, electrical conductivity, dielectric contrast and water content. Due to frequency-dependant attenuation mechanisms lower frequencies penetrate deeper than higher frequencies, but provide lower resolution. The depth of penetration in clays, namely in rocks with high conductivities is very limited (*Daniels, 2004; Jol, 2009*).

The objective of our study was to test the applicability and sensitivity of GPR and microgravity methods to identifying underground voids, such as cellars, in a complex urban environment. For this purpose we selected a cellar located under a private lot in a residential quarter of the district town of Senec in Western Slovakia that runs under the backyard and partially under the house of the lot.

2. The setting of the test case and the cellar

Pincesor, translated as "the quarter of cellars" is nowadays a residential suburb in the NW of Senec, built on lots formerly of poor habitations, over an area characterized by plentiful cellars, mostly wine cellars. The cellars were partly destroyed and partly covered by construction debris prior to building the new houses. Many of the cellars remain buried and unknown. This is why they may pose a threat to the infrastructure and inhabitants. The location of our survey area is shown in Fig. 1a.

The test cellar was discovered lately by chance, when a sinkhole developed after heavy rains in the yard just two metres away from the house and quite a lot of soil disappeared underground. After examining the sinkhole, a buried cellar was found. The owner excavated it and built an entrance, so it is easily accessible and can be used for storage now. This also allowed

us to position the cellar geodetically to create an approximate 3D model (plan view in Fig. 1b). It has a rectangular ground plan with dimensions of 11.3×2.8 m and height of 2.23 m. The vaulted ceiling of the cellar that runs under the backyard and partially under the house is located approximately 0.6 m below the ground.
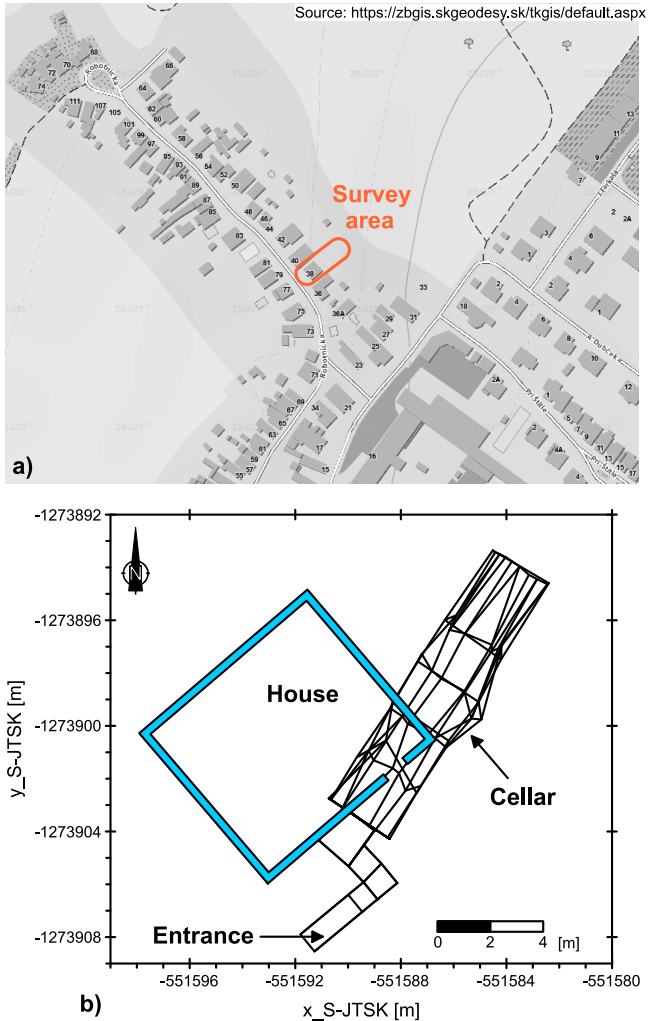
Fig. 1. Map of our survey area: a) private lot in the residential suburb Pincesor of Senec, southern Slovakia; b) plan view of the cellar running partially under the house.

A survey grid for GPR and microgravity observations was set up in the small backyard of the lot. The backyard is bounded by a technical room which serves as a wall for a steep terrain step 2.5 m high. The upper part behind this wall serves as a garden accessible by an external staircase cutting through the middle of the technical room (wall). The survey grid size (7 × 8 m) was enforced by the size of the lot bounded on the sides by fences. The neighbouring lots were not accessible to us. The GPR observations were performed in 3D configuration in the area marked by the red line in Fig. 2. The spacing between parallel GPR profiles was chosen at 0.5 m. The accessible area of the lot was covered by 84 microgravity observation points with an equidistant step of 1 m. The gravity stations were positioned geodetically.
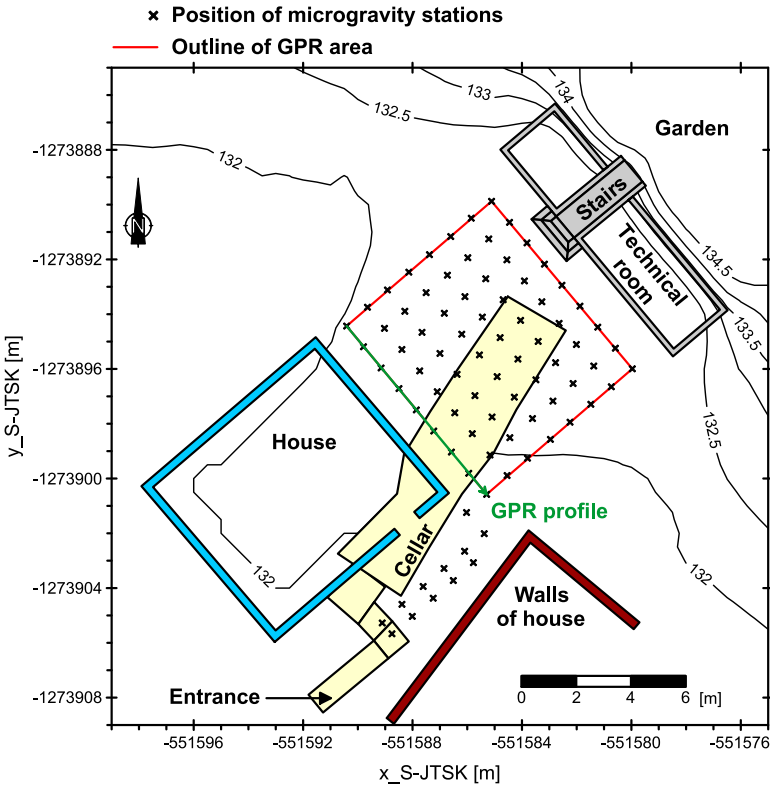
Fig. 2. Plot of the study area within the private lot together with contours of the digital elevation model.

The planimetric description was realized by a combination of GPS and total station (polar method) positioning. The following instruments were used: GPS antenna Leica Viva (with the average accuracy of 15.7 mm horizontally and 32.2 mm vertically achieved in situ); total station Sokkia SET230RK3 (angular accuracy $2''/0.6$ mg, accuracy in distance: a) in case of reflection prism: $\pm(2+2\,\text{ppm}*D)\,\text{mm}$, b) otherwise $\pm(3+2\,\text{ppm}*D)\,\text{mm}$, where D is baseline in km). Four reference points were fixed on the topographic surface of the lot using the RTK GPS approach (3 repeat observations at various stages). Some points of the survey grid were also positioned by this method. The position and 3D shape of the cellar was obtained by linking its positioning to the reference points via an oriented and closed polygon by means of the reflection-less polar mode total station observations.

3. GPR detection of the cellar

3.1. Instrumentation

The GSSI SIR-3000 system was used in order to carry out a ground penetrating radar (GPR) survey of the buried cellar. It is a lightweight, portable, single-channel GPR system that is ideal for a wide variety of applications. The main objective of the GPR investigation was to verify the position, size and shape of the known wine cellar buried under the private backyard. For this purpose an antenna with central frequency of 400 MHz and the measurement step of 0.005 m was employed. The measurement time record length of 80 ns was chosen, which was far over the manufacturer's recommended value. The standard setup including 1024 samples per scan, resolution of 16 bits, 3 gain points, vertical high pass filter (100 MHz) and vertical low pass filter (800 MHz) were used. The manufacturer's specified depth range for this type of antenna is about 3–4 m, which is sufficient for this kind of investigation. Radargrams were pre-processed by the special software package ReflexW (http://www.sandmeier-geo.de), a widely used geophysical near surface application software system. ReflexW is the DOS program for the processing and interpretation of reflection and transmission data designated for special applications such as GPR, ultrasound, reflection and refraction seismic.

3.2. Data acquisition and processing

The surface of the studied backyard was covered by a regular grid with the size of 8×9 m and spacing between parallel profiles set to 0.5 m (Fig. 2). Although the measurements were carried out in 3D configuration, the geological situation did not allow the interpretation of the whole grid as a 3D radargram. The data acquisition was carried out in situ by the above mentioned instrumentation and parameters. The profiles were measured twice during two days. The raw 2D data were first processed in the following manner: (1) application of the static correction, which adjusts the 0 value (the surface); (2) 2D filtration, which removes the background; (3) application of "Gain", which handles the energy decay, (4) performance of Complex trace analysis using the 1st derivative, and (5) 1D filtration using the band-pass butterworth filter, resulting in unwanted frequencies of less than 100 MHz and more than 800 MHz being filtered away.

These pre-processed data were subsequently interpreted. When the values of dielectric constant increased, positive peaks were considered as boundaries between layers, and *vice versa*. These peaks were detected semi-automatically in the ReflexW software package. In the end the obvious boundaries were interpreted and transformed to velocity models. The comparison of data traces from both days of measurement was carried out in Grapher by Golden Software (*Grapher, 2012*). Some special graphical operations were performed in Corel Draw (*Corel Draw, 2004*).

3.3. Interpretation

The backyard is covered prevailingly by lawn, and partially by a pavement. The lawn had been watered regularly prior to our field work. The geological situation (high clay content in the environment) and mainly regular watering of the lawn caused significant attenuation of the emitted GPR signal. For this reason, only 2D radargrams are presented here. Profiles running over the lawn produced unsatisfactory results. Only profiles running over the pavement part of the backyard yielded interpretable data. To show the effect of watering on the GPR investigation, we compare GPR profile data from the same profile for two consecutive days. Using the same view settings for both the days (Fig. 3), obvious differences can be observed by the naked eye. On the first measurement day, the signal is significantly attenuated,
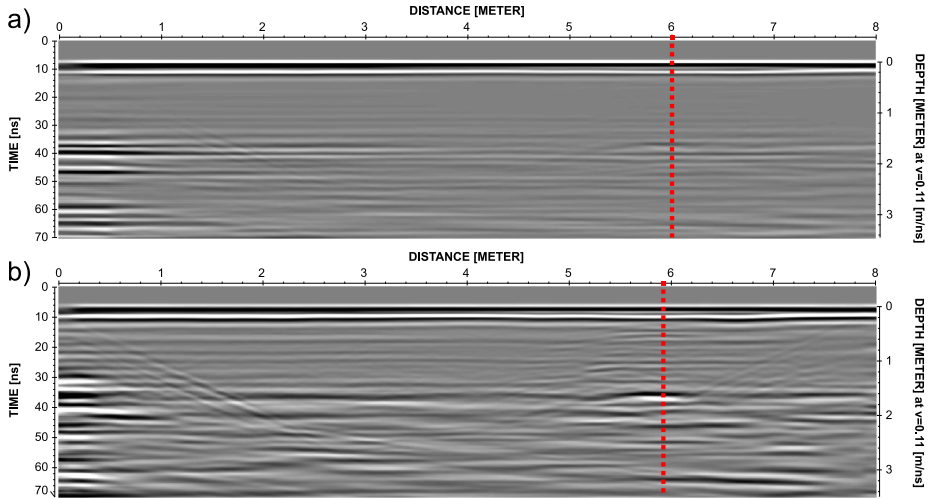
Fig. 3. Raw data from the first (a) and the second (b) days of GPR observations. Red dashed lines show the compared traces of the same profile line.

therefore only some indications of anomalies are visible. On the other hand, the second day brings much better data. These differences are caused by the different percentage of humidity in the studied soil and consequently by different signal attenuation.

Two traces were extracted from Fig. 3, from the same spot, compared and analysed. Comparing raw data from both measurement days, significant differences in amplitudes are evident (Fig. 4). It is possible to observe that the measurement from the second day shows higher peaks (difference of 45%), which could be assigned to a drier environment and better penetration of the signal through the soil. The only difference is the very first peak that is assigned to the boundary between air and soil. This may be caused by the bigger difference of the dielectric values on this boundary comparing these two days. Increased values of the constant probably result from the higher soil humidity in the first day of the GPR survey.

The GPR survey on the second day of our field work brought better quality data, as already mentioned. Only the profile running over the pavement (Fig. 2) was interpreted. The cross section was treated by mentioned processing flow and consequently interpreted. Fig. 5a shows the interpreted radargram with layers indicated by semi-automated interpreta-
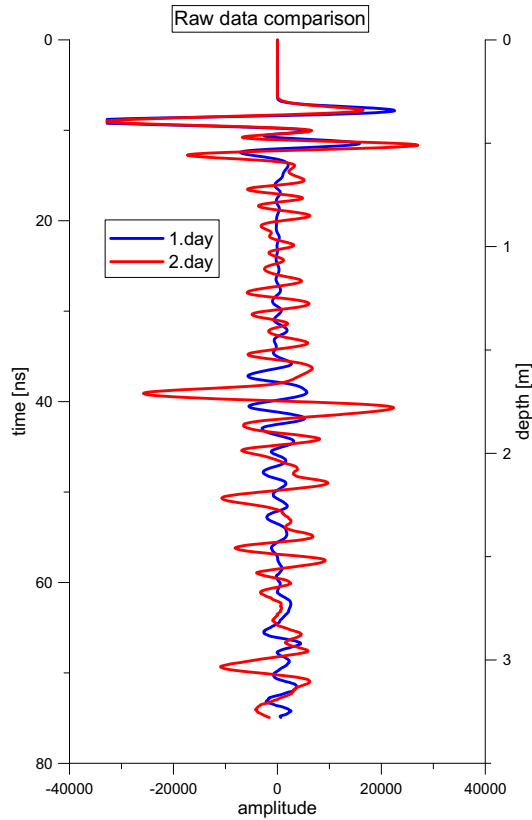
Fig. 4. Comparison of same traces at the same profile between two consecutive observation days.

tion. Coloured lines, yellow, brown and magenta, represent layers and the red one shows the bottom of the wine cellar. On the picture green and blue dashed lines can also be found. The green dashed lines show lateral reflections that originate probably from the concrete wall of the garden fence. The blue one is an interpretation of a boundary under the wine cellar. This reflection might represent the true wine cellar floor.

Fig. 5b shows the transformed velocity model of the studied cross-section. The studied environment is characterized by its electro-magnetic (elmag) parameters, from which the most important in most cases is the value of the dielectric constant. Since the environment is not homogenous, only an

21
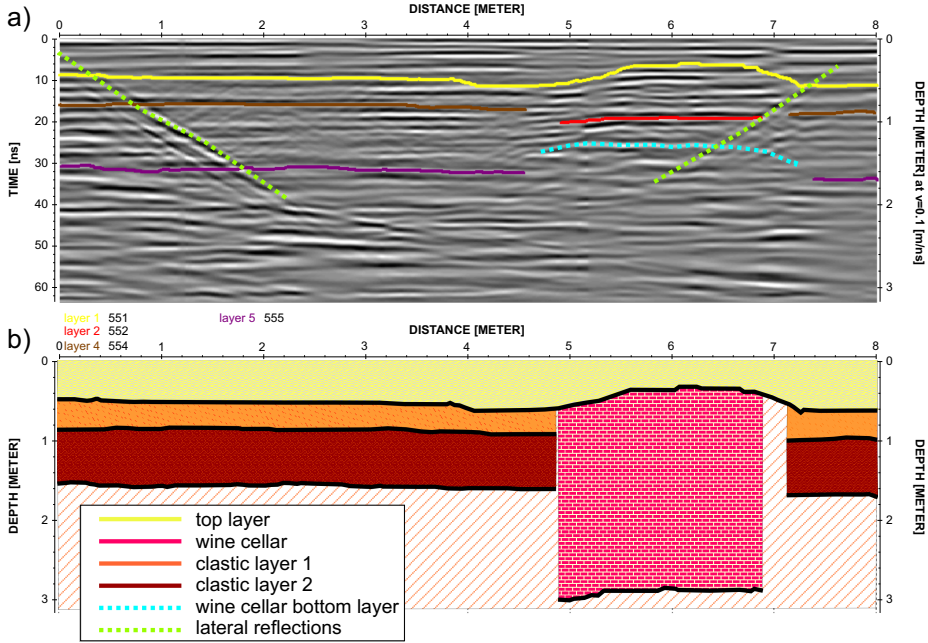
Fig. 5. The processed radargram with interpreted anomalies (a); the resulting transformed depth cross-section – layer view (b).

estimate of the average dielectric constant is taken into account. Every single layer is characterized by its own dielectric constant, and thus by its own velocity of the penetrating GPR (elmag) signal. Velocities and dielectric constants of the layers are shown in Table 1.

Table 1. Velocities and dielectric constants for each interpreted layer.

	velocity [m/ns]	dielectric constant
top layer	0.11	7.4
wine cellar	0.3	1.0
clastic layer 1	0.105	8.2
clastic layer 2	0.1	9.0

The top layer can be interpreted as a civil construction layer (earthwork) consisting of concrete pavement blocks and a gravel base. The next two layers may be formed by clastic material such as alluvial sediments. The

wine cellar is portrayed as a red bricks area in the right-side half of Fig. 5b. Since the whole wine cellar anomaly is not observed, only a part of it can be traced, although it is a bigger part.

4. Microgravity detection of the cellar

4.1. Instrumentation

Gravity measurements were taken at 84 points on the site, as shown in Fig. 2, by a Scintrex CG-5 Autograv gravimeter. This relative instrument based on a fused quartz spring balance with electrostatic nulling has a measurement range of 8000 mGal and a reading resolution of 0.001 mGal. Thanks to the use of low-noise electronic system for improved accuracy and speed of measurement, the gravity meter is suitable for both detailed microgravity surveys and large scale regional mapping (*Scintrex, 2006*). The horizontal location and elevations of gravity stations were determined using a total station SET230RK3 (Sokkia) with a sufficient accuracy in the Slovak National Coordinate System (Krovak projection S-JTSK). In addition a local coordinate system with starting point (50,200) and y-axis parallel to the house was chosen and used for the station numbering. To determine the gravimeter sensor elevation the distance between the ground level and the bottom of the instrument was measured and recorded at every station.

4.2. Data acquisition and processing

Gravity stations were measured during one day in a regular grid at 1 m spacing located in the backyard (Fig. 2). Two additional profiles were placed next to the house door aiming to map the continuation of the cellar in the narrow part of the lot. A fixed base station, established at a stable location outside the survey area, was reoccupied in a series of several readings each hour to monitor the residual instrument drift (i.e., to correct the gravity data for the temporal variations of the sensor). About 20% of the randomly selected stations were repeated during the survey to provide a repeatability control. An accuracy of ± 6 μGal based on a statistical analysis of these repeated measurements has been achieved. The gravity data were automatically corrected in the Autograv system for Earth tide variations, instrument

tilts, temperature changes and linear long term drift. The conversion of relative values to absolute gravity was not necessary because in microgravity surveys we are dealing only with the relative variations in the local gravity field.

The microgravity data were processed in a standard manner applying the residual drift, free-air, latitude, and planar Bouguer corrections. A correction density of 2.0 g/cm^3 was used in the calculation of the Bouguer anomaly. The latitudinal effects on the gravity stations were referenced to a base station (latitude of 48.2°) and calculated by assuming a linear gradient of the normal gravity field as a function of north-south distance (*Yule et al., 1998*). The estimated latitude correction was positive in our case because the stations are positioned south of the base station. Consequently the dataset was corrected for the gravitational effects of surrounding buildings and terrain.

The main walls of the owner's house are made of a Structural Insulated Panels (SIP) finished by plaster (density of 1.8 g/cm^3). It is a composite lightweight building material consisting of a rigid core sandwiched between two layers of structural board, in our case wood-based OSB panels (densities in a range of 0.58–0.72 g/cm^3). Either different types of foam or a mineral wool can be used as an insulation core. The densities of a mineral wool, which depends on fibre orientation, are defined in an interval 0.06–0.16 g/cm^3. An average correction density for the model of the house walls was estimated at 0.6 g/cm^3. The gravitational effects of a concrete slab and footings were calculated separately for densities of 2.4 g/cm^3 and +0.4 g/cm^3, respectively. The technical room located at the back of the yard is made of concrete blocks (a correction density of 2.2 g/cm^3). The last structures taken into account due to its proximity to the survey grid were two walls of an old neighbouring house (bricks, density of 1.9 g/cm^3), shown in Figs 2 and 6 by a dark red colour.

Fig. 6 provides an overview representation of all man-made structures used in the calculation of the building correction. Several colours were used in their visualization in order to distinguish between the different building materials they are made of. The buildings and the cellar were modelled manually as simple homogeneous polyhedral bodies in the PhotoModeler Scanner 6 software (http://www.photomodeler.com) using a set of main vertexes obtained from geodetic surveying. The building corrections of these mod-
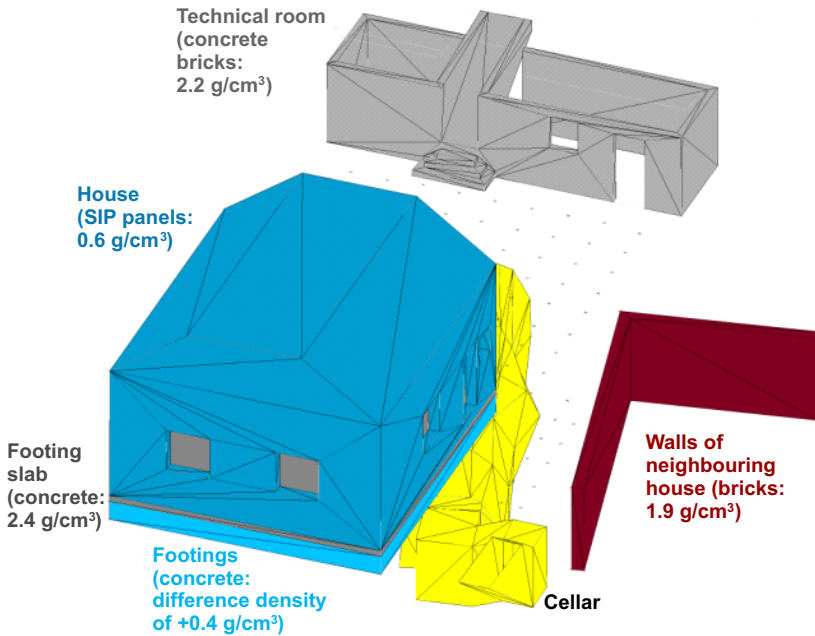
Fig. 6. Models of man-made structures made of different materials used in the calculation of the building correction.

els were calculated in program Polygrav (*Pánisová et al., 2012*) using the three-dimensional polyhedral body approximation of *Götze and Lahmeyer (1988)*. Bodies with different densities need to be imported and calculated separately. The amplitude of the cumulative building correction shown in Fig. 7a varies from 1 to 8 μGal nearest the brick house, which is comparable to the repeatability of microgravity measurements. The nearby buildings have minimal (almost negligible) disturbing effect on the gravitational signature of the sought target.

The terrain correction is a strong function of distance. The nearest topographic features have the greatest influence because of the inverse square low of gravity (*Long and Kaufmann, 2013, p. 30*). Therefore only the inner zone terrain correction up to a 250 m distance was calculated in software TopoSK (*Marušiak and Mikuška, 2013*) for a density of 2.0 g/cm^3 using the available digital elevation model with a grid spacing of 1 m supplemented with additional topographic data from a parallel geodetic survey.
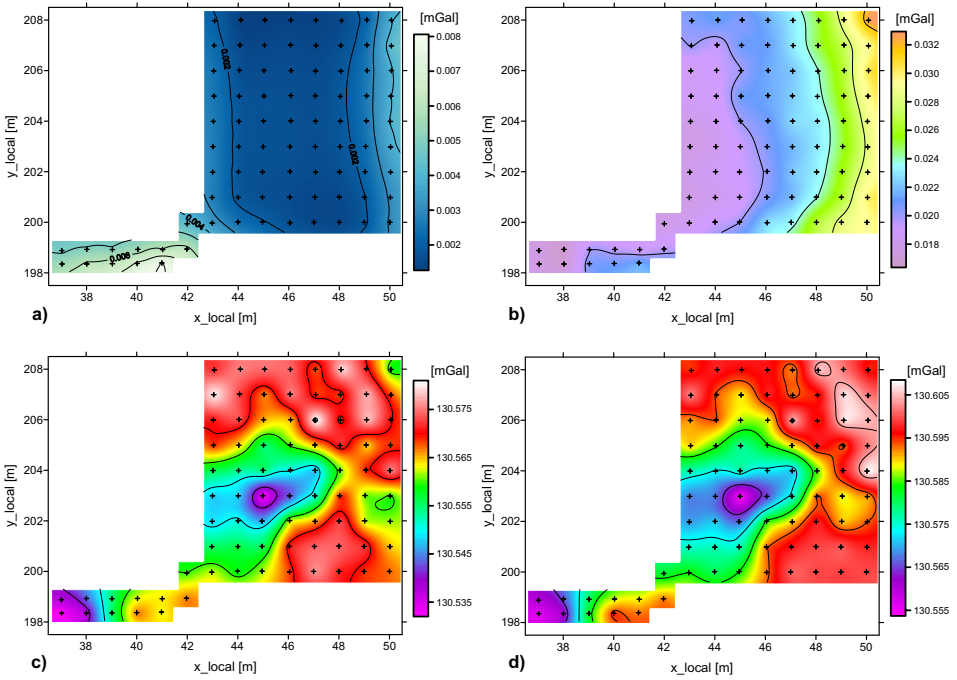
Fig. 7. Cumulative building correction (a); Terrain correction up to 250 m (b); Simple Bouguer anomaly (c); Complete Bouguer anomaly after applying terrain and building corrections (d).

Due to the small dimensions of the survey area and small height differences among acquisition points the terrain corrections for distant zones could be neglected. The terrain correction displayed in Fig. 7b takes into account the main topographic feature on the site, namely a 2.5 m high steep elevation jump behind the technical room from the backyard to the garden level. The terrain correction has a non-linear character, with maximal amplitude of 32 μGal in the vicinity of the technical room, decreasing in the direction of the owner's house to 16 μGal.

Visual comparison of the simple Bouguer anomaly map (Fig. 7c) with the complete Bouguer anomaly map after eliminating the effects of natural and man-made topographic variations (Fig. 7d) suggests that the terrain and building corrections have influenced the shape of the Bouguer anomaly only slightly. The presence of the known test cellar is indicated by a distinc-

tive gravity low easily identifiable and dominating already on the simple
Bouguer anomaly map in Fig. 7c. The final applied processing step was
the separation of regional and residual gravity. A second degree polyno-
mial (a regional trend) was fitted and removed from the data. The residual
Bouguer anomaly map shown together with the ground plan of the house
and the cellar in Fig. 8a was used in the interpretation.

4.3. Interpretation

Due to the accessibility issues caused by the presence of several buildings
on the survey site, the negative anomaly produced by the test cellar could
be only partially traced by the microgravity method (Fig. 8a). Qualitative
interpretation of the truncated negative anomaly of amplitude higher than
-60 μGal indicates the narrow and elongated shape of the cellar that is
heading from the house towards the stairs to the garden. The gravitational
effect of the empty cellar model, which consists of 146 triangles, was com-
puted in program Polygrav for a zero density. The calculated map of the
cellar effect was blanked to the extent of the microgravity grid (Fig. 8b).

Fig. 9a shows the difference map between the observed residual anoma-
lous (Fig. 8a) and calculated (gravitational effect of the cellar; Fig. 8b)
gravity fields of the test cellar. The remaining model misfit is probably due
to the random measurement errors of individual points combined with the
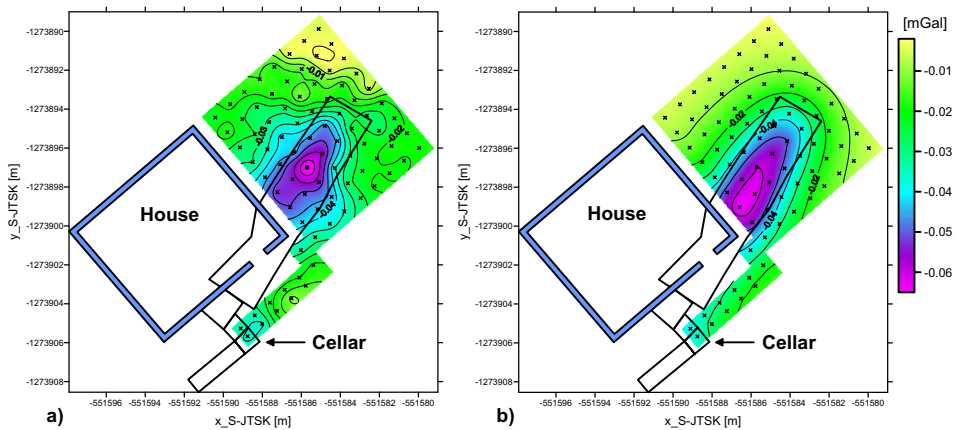
Fig. 8. Residual Bouguer anomaly (a); Gravitational effect of the modelled cellar (b).

background noise (effects) from all other anomaly sources. These combined effects partially deform the main negative anomaly of the residual gravity map displayed in Fig. 8a. The sources of the man-made noise are the shallowest density heterogeneities that were created by the redevelopment of the yard when the area was filled by low density rubble.

In order to validate the depth of the test cellar we have used the 3D
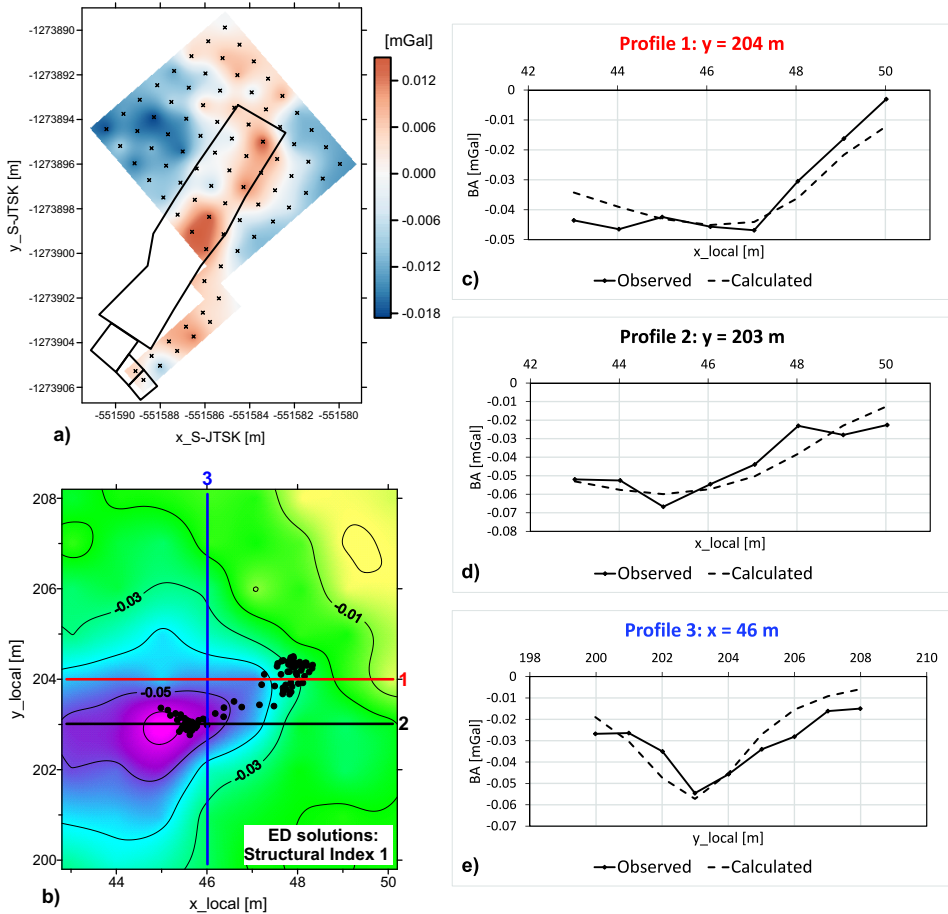
Fig. 9. (a) Map of the difference between the residual Bouguer anomaly (Fig. 8a) and the gravitational effect of the cellar (Fig. 8b); (b) the interpretation by 3D Euler deconvolution method (SI = 1; horizontal cylinder in gravimetry); (c)–(e) comparison of the observed and calculated gravity for profiles 1–3.

Euler deconvolution. Euler deconvolution (ED) of potential fields is one of the semi-automated interpretation methods, by which possible source depths from gravity and magnetic anomalies are determined based on both their amplitudes, gradients and an estimate of the probable geometry of the causative structure (*Reid et al., 1990*). We used an in-house program Regder developed at the Comenius University in Bratislava. During the calculation a window of specific size is moved across the gridded data, using least-square inversion, to solve Euler's homogeneity equation with regularized derivatives incorporated (*Pašteka et al., 2009*).

To help distinguish the type of the anomalous target two structural indices (SI) related to the fall-off rate of the anomaly were chosen: i) detecting a horizontal cylinder (SI = 1) and ii) detecting a sphere (SI = 2). The locations of the ED solution clusters in the area of the main gravity low are almost identical in both cases with the similar degree of clustering. Therefore only the selected solutions for the structural index one are shown by filled black circles in Fig. 9b. When detecting spherically shaped bodies (SI = 2 in gravimetry), the average depths of the ED solution clusters fell within the range of 1.6–2.3 m. The choice of structural index one leads to lower values of the solution clusters depth in the range of 1.0–1.6 m below the ground in comparison with the centre of the geodetically measured cellar (approx. depth of 1.7 m).

In graphs (c)–(e) on the right side of Fig. 9 the observed and calculated gravity fields are compared. The location of the three profiles is depicted in the local coordinate system of Fig. 9b by different colours. Figures 9c–9e show reasonable fit between the modelled and measured fields in the central part of the negative anomaly. Considering the small depths of the top of the test feature (~ 0.6 m) the approximate cellar model created on the basis of the conventional geodetic measurements (coloured yellow in Fig. 6) might be insufficient for our purposes. The terrestrial laser scanning would be a more suitable surveying method for more realistic reconstruction of the cellar's topology.

5 Discussion and conclusions

The GPR survey was conducted during two days. Comparing the data acquired during these two days, a significant difference can be observed. It

is mainly the quality of data influenced probably by the watering of the lawn. The humidity of the geological environment attenuates the electromagnetic GPR signal. For this reason only the profile running over the concrete pavement was interpreted. Although the GPR investigation has some limitations of use due to its principles of operation, it can still serve as a useful geophysical method for fast and effective detection of underground voids.

The total width of a microgravity survey should extend beyond the observable gravitational effect of the target structure. In our case this condition could not be met due to accessibility issues. This led to some difficulties in identifying the long-wavelength regional field component in the measured gravity field. Under such circumstances any further quantitative analysis of the anomaly (an amplitude of -66 μGal) by means of direct or inverse interpretation methods was not plausible. Both tested structural indices in the 3D Euler deconvolution provided reasonable depth estimates of the studied cellar, namely estimates of the center of 1.3 m (SI = 1), 1.95 m (SI = 2) versus 1.7 m from geodetic measurements. The deviation between the gravitational effect of the cellar and the residual gravity field is likely due to: i) the density inhomogeneity of the sediment fill; ii) the complexity of the urban surroundings; and iii) the residual-regional field separation used. Despite these limitations we can conclude that the test cellar has been successfully detected by the microgravity method.

Our combined GPR and microgravity survey was carried out over a selected test cellar located in a densely populated area of the town of Senec. Compared to GPR the microgravity method is more time consuming as a high accuracy of the gravity measurements is required. This is directly related to the accuracy of vertical positioning. Consequently, the elevation of each gravity station has to be precisely acquired by geodetic surveying methods. In addition, gravimeters are extremely sensitive devices that are affected by any local source of vibrations. On the other hand, microgravity methods may succeed in almost any urban site conditions where other geophysical methods could fail due to several factors, such as soil moisture, precipitation, or electromagnetic noise. The only two conditions to be satisfied are i) a sufficient density contrast of the detected target with respect to the surrounding host rock and ii) an appropriate ratio of the depth of burial to its size.

This case study proves that geophysical prospection is suitable for detection of unknown underground voids even in complex urban settings. Compared to the threat and potential costs of damages caused by subsidence or caving-in in urban areas undermined by unknown void spaces or structures, the cost and speed of execution of the two discussed approaches to the geophysical prospection is definitely worth the effort.

References

Al-Rifaiy I. A., 1990: Land subsidence in the Al-Dahr residential area in Kuwait: a case history study. Quarterly Journal of Engineering Geology and Hydrogeology, **23**, 337–346.

Banham S. G., Pringle J. K., 2011: Geophysical and intrusive site investigations to detect an abandoned coal-mine access shaft, Apedale, Staffordshire, UK. Near Surface Geophysics, **9**, 483–496.

Cardarelli E., Cercato M., Cerreto A., Di Filippo G., 2010: Electrical resistivity and seismic refraction tomography to detect buried cavities. Geophysical Prospecting, **58**, 685–695.

Corel Draw, Version 12, 2004, Corel Corporation, USA, Canada. Reflex-Win PreVersion 7.0, 1997–2012, Sandmeier software, Karlsruhe, Germany.

Daniels J., 1988: Locating caves, tunnels and mines. Geophysics: the Leading Edge, **7**, 32–37 and 52.

Daniels D. J., 2004: Ground penetrating radar, 2nd edition. Published by the Institution of Electrical Engineers, London, United Kingdom. p. 734.

Götze H. J., Lahmeyer B., 1988: Application of three-dimensional interactive modeling in gravity and magnetic. Geophysics, **53**, 1096–1108.

Grapher, Version 9, 2012, Golden Software, Colorado, USA. SIR System – 3000 Manual, 2011, Geophysical Survey Systems, Inc, New Hampshire, USA.

Jol H. M., 2009: Ground Penetrating Radar: Theory and Applications. Elsevier Science Amsterdam, First edition 2009, p. 508.

Long L. T., Kaufmann R. D., 2013: Acquisition and Analysis of Terrestrial Gravity Data. Cambridge University Press, Cambridge UK, p. 171.

Marušiak I., Mikuška J., 2013: Toposk – software for terrain corrections evaluation. Manual, G-trend Ltd., Bratislava, manuscript, 1–12 (in Slovak).

Negri S., Margiotta S., Maria Quarta T. A., Castiello G., Fedi M., Florio G., 2015: Integrated analysis of geological and geophysical data for the detection of underground man-made caves in an area in southern Italy. Journal of Cave and Karst Studies. **77**, 52–62.

Pánisová J., Pašteka R., Papčo J., Fraštia M., 2012: The calculation of building corrections in microgravity surveys using close range photogrammetry. Near Surface Geophysics, **10**, 391–399.

Pašteka R., Richter P., Karcol R., Brazda K., Hajach M., 2009: Regularized derivatives of potential fields and their role in semi-automated interpretation methods. Geophysical Prospecting. **57**, 507–516.

Reid A. B., Allsop J. M., Granser H., Millett A. J., Somerton I. W., 1990: Magnetic interpretation in three dimensions using Euler deconvolution. Geophysics, **55**, 80–91.

Scintrex, 2006: CG-5 Scintrex Autograv System, Operation Manual, 2006: Ontario, Canada. Scintrex Limited, Nr. 867700 Rev. 4, p. 308.

Styles P., McGrath R., Thomas E., Cassidy N. J., 2005: The use of microgravity for cavity characterization in karstic terrains. Quarterly Journal of Engineering Geology and Hydrogeology, **38**, 155–169.

Styles P., Toon S., Thomas E., Skittrall M., 2006: Microgravity as a tool for the detection, characterization and prediction of geohazard posed by abandoned mining cavities. First Break 2, **4**, 51–60.

Tuckwell G., Grossey T., Owen S., Stearns P., 2008: The use of microgravity to detect small distributed voids and low-density ground. Quarterly Journal of Engineering Geology and Hydrogeology, **41**, 371–380.

Yule D. E., Sharp M. K., Butler D. K., 1998: Microgravity investigations of foundation conditions. Geophysics. **63**, 95–103.